JOURNAL OF MAGNETIC RESONANCE **132,** 274–278 (1998)
ARTICLE NO. MN981412

NMR Imaging Using Second Order Quadrupole Broadened Resonances

V. Srirama Swaminathan and B. H. Suits[1]

Department of Physics, Michigan Technological University, 1400 Townsend Drive, Houghton, Michigan 49931

Received May 20, 1997; revised February 3, 1998

Theoretical and experimental results for NMR imaging measurements of powdered materials using the $+\frac{1}{2}$ to $-\frac{1}{2}$ transition of $\frac{1}{2}$-integer spin nuclei in the presence of a very large second-order electric quadrupolar broadening are presented. An "effective spin-$\frac{1}{2}$" formalism is developed to account for additional effects due to the presence of quadrupolar interactions comparable in size to the Zeeman interaction. A large (7.9 mT/cm-A, with a maximum current of ≈20 A), rapid (≈30 μs) pulsed linear gradient field is used with echoes and phase encoding techniques to obtain images in the limit γH_1 is much narrower than the NMR linewidth. A one-dimensional projection of the second-order quadrupolar perturbed, 4-MHz-wide, $+\frac{1}{2} \leftrightarrow -\frac{1}{2}$ transition for ^{63}Cu in Cu_2O powder is presented as an example. An experimental one-dimensional projection of a sample containing Cu_2O and $YBa_2Cu_3O_{6.7}$ is also presented.

INTRODUCTION

NMR imaging studies using the signal from $\frac{1}{2}$-integer nuclei in quadrupole perturbed systems have used the fact that the broadening of the central transition ($+\frac{1}{2}$ to $-\frac{1}{2}$) is affected only to second order (*1*). In the systems studied the central transition remained narrow enough so that relatively straightforward imaging techniques (*2–5*) could be employed. In this work we examine the limit of large quadrupole coupling on imaging capabilities.

The powder linewidth of the central transition of a $\frac{1}{2}$-integer quadrupolar nucleus in a solid can range from less than 1 kHz to many megahertz. The linewidth due to electric field gradients (EFGs) is determined by the ratio of the quadrupole coupling constant, ν_Q, to the Larmor frequency, ν_L (*1, 6, 7*). The effects of the EFG on the NMR spectrum can be used to study symmetry and stoichiometry variations, defects (*3*), and other forms of disorder within a sample (*8, 9*). In what follows, the utility of using standard NMR imaging measurement techniques with readily available gradient and RF strengths for very wide NMR lines is examined.

The field gradients typically used for NMR imaging are a small perturbation of the much larger Zeeman interaction from the static magnetic field. Because of this, only the components from the magnetic field gradient which are along the static field need to be considered. In the presence of a large EFG interaction, the quantization axis is no longer along the static field, but will be along a direction determined by the combined Zeeman and electric quadrupole interactions. A gradient coil must always produce magnetic fields in directions perpendicular to the static field (*10, 11*), and hence those perpendicular fields may become important for the present case. We use second-order perturbation and an "effective spin-$\frac{1}{2}$" formalism (*1*) to estimate the size of the effects of the components of the field gradients which are perpendicular to the static magnetic field in the presence of a large EFG.

We used a simple phase encoding (*12*) imaging technique, appropriate for inhomogeneously broadened lines, to produce a one-dimensional projection of a broad line material both numerically and experimentally. Two experimental images are presented. One image is obtained using the 4-MHz-wide, $+\frac{1}{2} \leftrightarrow -\frac{1}{2}$ transition of ^{63}Cu in Cu_2O powder, and the other is a combination of a 9-MHz-wide $YBa_2Cu_3O_{6.7}$, a high-temperature superconducting (HTSC) powder, and diluted Cu_2O powder.

THEORY

Effective Spin-$\frac{1}{2}$ Formalism

For $\frac{1}{2}$ integer nuclei in powdered materials and in the presence of a large electric quadrupole coupling, the $\pm\frac{1}{2} \leftrightarrow \pm\frac{3}{2}$ and other satellite transitions will be shifted to first order and will be unobservable. Here we calculate the behavior of the $+\frac{1}{2} \leftrightarrow -\frac{1}{2}$ transition, shifted in second order and in the presence of the magnetic field gradients used for imaging. The following calculations are restricted to the case where the electric quadrupole interaction is axial, $\eta = 0$, and $I = \frac{3}{2}$. The extension of the technique to the more general case is tedious, though straightforward.

The Hamiltonian of a spin system with a quadrupole interaction in a magnetic field H along the z-axis in the laboratory reference frame, and in the presence of the magnetic field gradients used for imaging, is given by

$$\mathcal{H} = \mathcal{H}_{\mathcal{M}} + \mathcal{H}_{\mathcal{Q}} + \mathcal{H}_{\mathcal{G}} \qquad [1]$$

where $\mathcal{H}_{\mathcal{Q}}$ is the Hamiltonian due to the quadrupole interaction, $\mathcal{H}_{\mathcal{G}}$ is the Hamiltonian due to the applied magnetic field gradients, and

$$\mathcal{H}_{\mathcal{M}} = -\gamma\hbar H_o I_z \qquad [2]$$

is the Zeeman Hamiltonian.

[1] To whom correspondence should be addressed.

1090-7807/98 $25.00

We use x, y, and z to define the laboratory reference frame and X, Y, and Z to define the principal axes of the EFG. Since an axial EFG is assumed here, only two polar angles, θ and ϕ, are needed to specify the relative orientation of these reference frames. The angle between Z and z, θ, is sufficient to determine the energy-level splitting in the absence of the magnetic field gradients. The angle ϕ is defined so that when $\phi = 0$, z is in the X–Z plane.

In terms of the operators I_x, I_y, and I_z in the lab frame, the quadrupole Hamiltonian is (*1*)

$$\begin{aligned}\mathcal{H}_Q(\theta, \phi) = &\frac{\nu_Q}{6}\left[\frac{1}{2}(3\mu^2 - 1)(3I_z^2 - a)\right] \\ &+ \frac{\nu_Q}{6}\left[\frac{3}{2}\mu\sqrt{1-\mu^2}\,[(I_zI_+ + I_+I_z)e^{-i\phi} \right. \\ &\left. + (I_zI_- + I_-I_z)e^{i\phi}]\right] \\ &+ \frac{\nu_Q}{6}\left[\frac{3}{4}(1-\mu^2)(I_+^2 e^{-2i\phi} + I_-^2 e^{2i\phi})\right], \end{aligned} \quad [3]$$

where $\mu = \cos\theta$ and $a = I(I+1)$.

The gradient term is given by

$$\mathcal{H}_G = \sum_{a,b=x,y,z} -\gamma I_a G_{ab} x_b \quad [4]$$

where $G_{ab} = \partial H_a/\partial b|_0$, $a, b = x, y, z$. Using time-independent perturbation theory for nondegenerate spins (*13*), the nuclear spin wavefunctions are calculated to second order in ν_Q/ν_L in the absence of a gradient.

Using these second-order wavefunctions, matrix elements for the operators I_x, I_y, and I_z are calculated. Since we are only looking at two levels, $m = \pm\frac{1}{2}$, one can write the Hamiltonian in terms of spin-$\frac{1}{2}$ operators I_x', I_y', and I_z' to get an ''effective spin-$\frac{1}{2}$'' Hamiltonian (to second order)

$$\mathcal{H} = \epsilon I_z' + \text{const}, \quad [5]$$

where ϵ is the energy splitting between the states. Using the perturbed wavefunctions and keeping only those terms involving I_z', $\mathcal{H}_G$ is found to be

$$\begin{aligned}\mathcal{H}_G = &-\gamma I_z'\left[G_{zx}x + G_{xz}z\cos\phi\,\frac{3\mu\sqrt{1-\mu^2}\,(9\mu^2-5)}{4}\,\frac{\nu_Q^2}{\nu_L^2}\right] \\ &- \gamma I_z'\left[G_{yz}z\sin\phi\,\frac{3\mu\sqrt{1-\mu^2}\,(9\mu^2-5)}{4}\,\frac{\nu_Q^2}{\nu_L^2}\right] \\ &+ \gamma I_z'\left[G_{zx}x\,\frac{(153\mu^4 - 162\mu^2 + 9)}{64}\,\frac{\nu_Q^2}{\nu_L^2}\right]. \end{aligned} \quad [6]$$

For simplicity, a simple ideal saddle gradient coil designed to produce $G_{xz} = G_{zx} = dH_z/dx \neq 0$, with the remaining gradient terms zero, is considered (*10*). The resulting effective gradient magnetic field can be written in the form

$$H(x, y, z) = G_{zx}\left[x + \frac{\nu_Q^2}{\nu_L^2}(a_x x + a_z z)\right], \quad [7]$$

where

$$a_x = \frac{(153\mu^4 - 162\mu^2 + 9)}{64}$$

$$a_z = \cos\phi\,\frac{3\mu\sqrt{1-\mu^2}\,(9\mu^2-5)}{4}.$$

In the absence of the gradient, the NMR frequency for a particular crystallite in the powder sample will depend only on θ. With an applied gradient, the frequency becomes a complicated function of the crystallite's position and orientation.

When the RF excitation, γH_1, is small compared to the second-order powder linewidth, only those nuclei near the excitation frequency, ω, respond. Hence, for any particular choice of excitation frequency only nuclei from crystallites at a small set of values of θ will contribute. For each of these values of θ, all possible values of ϕ occur with equal probability. When averaged over all ϕ, the angular-dependent terms average to zero and hence the correction terms will not give rise to net shift of the NMR intensity. The correction terms will give rise to a broadening, which reduces the ultimate resolution in the image.

To estimate the extent of the broadening, a sample consisting of a thin disc of radius r, with its axis along the x-direction and in the plane $x = x_o$, is considered. With a time-independent gradient and considering only those nuclei oriented at (θ, ϕ), a measured 1D projection as a function of position and frequency shift $\Delta\omega'$ will be given by

$$\begin{aligned} S(x_o, \Delta\omega') &= \frac{r}{\gamma a_z(\nu_Q^2/\nu_L^2)}\sqrt{1-\alpha^2}, \quad -1 < \alpha < 1 \\ &= 0 \text{ otherwise}, \end{aligned} \quad [8]$$

where

$$\alpha = \frac{1}{ra_z}\left[\left(\frac{\Delta\omega'}{\gamma G_{zx}} - x_o\right)\frac{1}{(\nu_Q^2/\nu_L^2)} - a_x x_o\right].$$

In the limit where $\nu_Q = 0$, $S(x_o, \Delta\omega')$ is a delta function $\delta(\Delta\omega' - \gamma G_{zx}x_o)$, and the usual NMR imaging result is obtained.

Recognizing that $\langle a_x^2\rangle \approx 1$, and with $x_o \leq r$, the extra broadening due to the presence of the EFG will be $\gamma G_{zx} r\nu_Q^2/\nu_L^2$, within factors of order of unity. The ultimate resolution will then be proportional to the size of the sample.

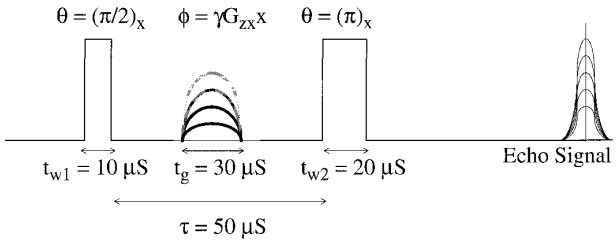

FIG. 1. Diagram of the echo pulse sequence used in 1D phase encoded imaging. The figure is not drawn to scale.

Image Profile Calculation

Walstedt (*14*) provides a formalism to calculate the results of a two-pulse spin echo for inhomogeneously broadened NMR lines in solids. We extend this formulation to accommodate a simple one-dimensional pulsed gradient to yield a phase encoded image. We assume that γH_1 is much smaller than the NMR linewidth and the relaxation effects are negligible. A two pulse echo sequence with a gradient pulse placed between two RF pulses (Fig. 1) is used. It is assumed that all the pulses are of short duration.

The gradient pulse, of duration t_g, is added and modeled using a rotation about the z-axis. We write $G_{xz} = G_{zx} = \alpha g_o$ where α is a unitless real number. Experimentally, g_o will be the smallest gradient strength used and α will take on integer values. Following Walstedt's procedure and evaluating the received echo signal at $t = 2\tau$, we find for a cylindrical sample of unit radius and length $2x_o$,

$$S_x(\beta) \simeq \sum_n \int_0^{2\pi} d\phi \int_{-\infty}^{\infty} d\omega' \int_{-x_o}^{x_o} dx\, g(\omega') \frac{1}{a_z(\nu_Q^2/\nu_L^2)} \times \sqrt{1 - \frac{1}{a_z^2}\left[\left(\frac{\beta}{\gamma g_o t_g} - x\right)\frac{1}{\nu_Q^2/\nu_L^2} + a_x x\right]^2} \times [\rho \cos(\Delta\omega t_g) - \sigma \sin(\Delta\omega t_g)], \quad [9]$$

where $g(\omega')$ is the NMR powder lineshape, $\Delta\omega = \omega' - \omega$, $\rho = R_{13}(R_{11} - R_{22})$, $\sigma = R_{23}(R_{11} - R_{22})$, with R_{ij} given in (*14*). The sum is over the different values of θ which contribute to the lineshape at ω. In the absence of an EFG, the unitless parameter β can be directly interpreted as position in units of $1/\gamma g_o t_g$, and $S(\beta)$ is a 1D projection of the sample.

EXPERIMENTAL

A homebuilt spectrometer, built around an 8.47-T superconducting wide-bore magnet, was used for imaging. A linear gradient was generated using a fully automated gradient circuit based on Conradi *et al.*'s design (*15*). With the components used, this circuit resulted in a current pulse of width ≈30 μs in the form of half of a sinusoidal. The peak current through the gradient coil during one cycle is about 20 A. A simple Golay–Saddle coil (*10, 16, 17*) designed to produce a linear gradient with $\partial H_z/\partial x \neq 0$ was used. The coil we used was 8-mm-diameter, 24-turn, 30-gauge copper wire with $L_{parallel} = 30\ \mu$H and $R_{dc} = 1.2\ \Omega$. We could obtain a gradient of 7.9 mT/cm-A (339 kHz/cm-A for protons) with this circuit and this coil configuration. The length of the linear region along the axis was measured to be 1.4 cm.

Powdered Cu_2O was used for most measurements. The ^{63}Cu nucleus in Cu_2O experiences a strong nuclear electric quadrupole interaction with a quadrupole coupling constant ν_Q = 26.97 MHz and $\eta = 0$ (*18*). This results in a powder linewidth of 4 MHz for the $+\frac{1}{2} \leftrightarrow -\frac{1}{2}$ transition as shown in Fig. 2.

Limited measurements were made using a sample of $YBa_2Cu_3O_{6.7}$, a high-temperature superconducting material with an oxygen-deficient perovskite-like structure in which the oxygen vacancies are ordered. There are two copper sites in this structure: The Cu1 ion sites are at the center of an oxygen rhombus-like square and the Cu2 ion is five-coordinated by an apically elongated pyramid. The quadrupole coupling constant ν_Q of the ^{63}Cu nucleus is 38.2 MHz in Cu1 chains and 62.8 MHz in Cu2 planes, and in both cases $\eta \neq 0$ (*19*). This quadrupole interaction results in a powder linewidth of about 9 MHz.

Room-temperature, 1D phase encoded projections of the spin density were obtained for two different phantoms of powdered Cu_2O and a phantom made out of $YBa_2Cu_3O_{6.7}$ powder and diluted Cu_2O. A Hahn echo pulse sequence with a single gradient pulse applied between the $\frac{\pi}{2}$ (10 μs) and π (20 μs) pulses was employed. The π pulse was applied 50 μs (τ) after the $\frac{\pi}{2}$ pulse. Because of the low signal-to-noise ratio, 64,000 acquisitions were averaged for each echo. Though not pursued here, the use of slow sample rotation during the measurement could be used to decrease the total acquisition time (*20, 21*). The echo signals as a function of gradient strength were stored and the image was reconstructed from the resulting pseudo FID using a fast Fourier transform. Measurements presented here were made at 96.2 MHz, which is sufficiently far from the Knight shifted ^{63}Cu signal from the copper gradient and RF coils so that no interference from the coils is seen. At this frequency, crystallites oriented with θ = 11.5, 65.4, 111.5, and 161.5° contribute to the lineshape.

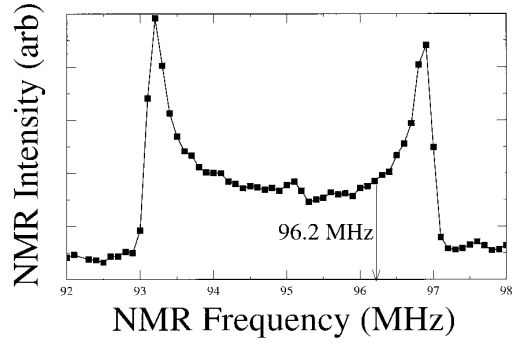

FIG. 2. NMR spectrum of central ($+\frac{1}{2} \leftrightarrow -\frac{1}{2}$) transition for ^{63}Cu in Cu_2O powder. Here ν_Q^2/ν_L^2=0.0738. Imaging measurements were made at 96.2 MHz.

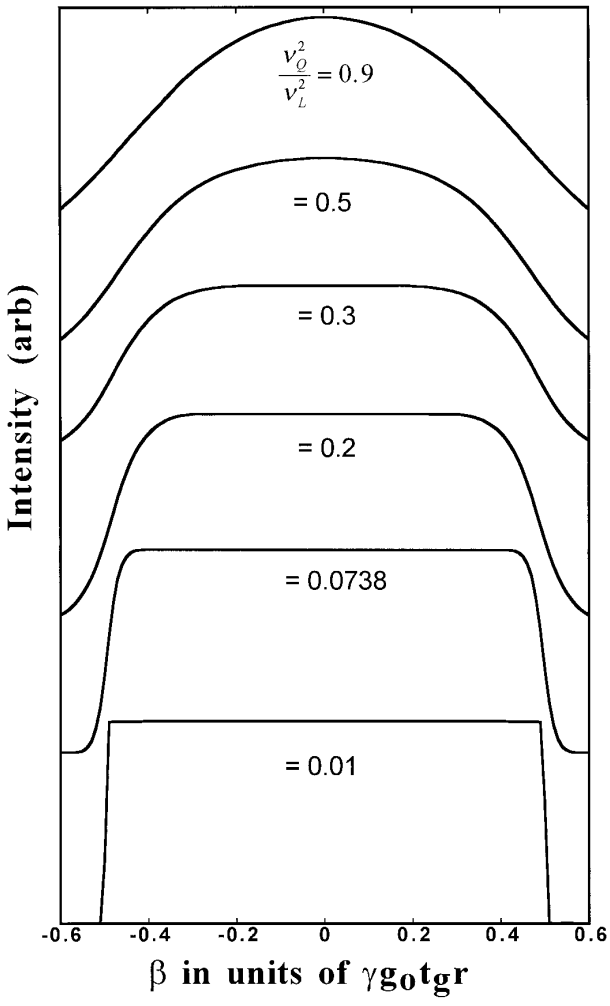

FIG. 3. Simulated phase-encoded 1D projections for cylinder of unit length and radius for $\nu_Q^2/\nu_L = 0.01$, 0.0738, 0.2, 0.3, 0.5, and 0.9 at $\theta = 11.5$, 65.4, 111.5, and 161.5° corresponding to the frequency 96.2 MHz. This simulation is done using Eq. [9].

RESULTS AND DISCUSSION

Numerical simulations using Eq. [9] were made for a variety of values of ν_Q^2/ν_L^2, including 0.0738, which is appropriate for our Cu_2O measurements, and with $g(\omega') =$ constant, appropriate for very broad lines. For these idealized simulations, the only broadening is that due to the powder average in the presence of the EFG. Values of ν_Q^2/ν_L^2 up to 0.9 are presented in Fig. 3, though for larger values second-order perturbation theory may not be entirely accurate. Nevertheless, when $\nu_Q^2/\nu_L^2 \geq 0.5$, the image resolution will be comparable to the size of the sample and the simple technique used here would not produce good results. For our Cu_2O measurements, however, the broadening is predicted to be small and other sources of broadening can be expected to dominate, typical of the broadening seen in other solids, at least for small samples.

Several measurements were made to show that images can be obtained for severely broadened NMR lines. Experimental one-dimensional projections of a 5-mm-diameter cylindrical sample for 9.5-mm single and 8.6-mm two-piece Cu_2O powder samples are shown in Figs. 4a and 4b. For the sample used to obtain the data in Fig. 4b, the Cu_2O powder occupies two cylindrical regions each 2.3 mm long with a 4-mm gap. An experimental one-dimensional projection of a sample including HTSC and Cu_2O (diluted with chalk dust) is shown in Fig. 4c. The entire sample is 12 mm long, the HTSC, 6.1 mm long, and the diluted Cu_2O, 4.9 mm long. A Teflon cap 1 mm long is placed between the HTSC and Cu_2O mixture. The different densities of ^{63}Cu, different relaxation times, and differing lineshapes result in very different image intensities for the two materials. The observed intensities agree with values calculated taking these effects into account. This material-specific contrast, which will depend on the frequency chosen for the measurement, may be useful for identifying the spatial distribution of different materials within an inhomogeneous sample.

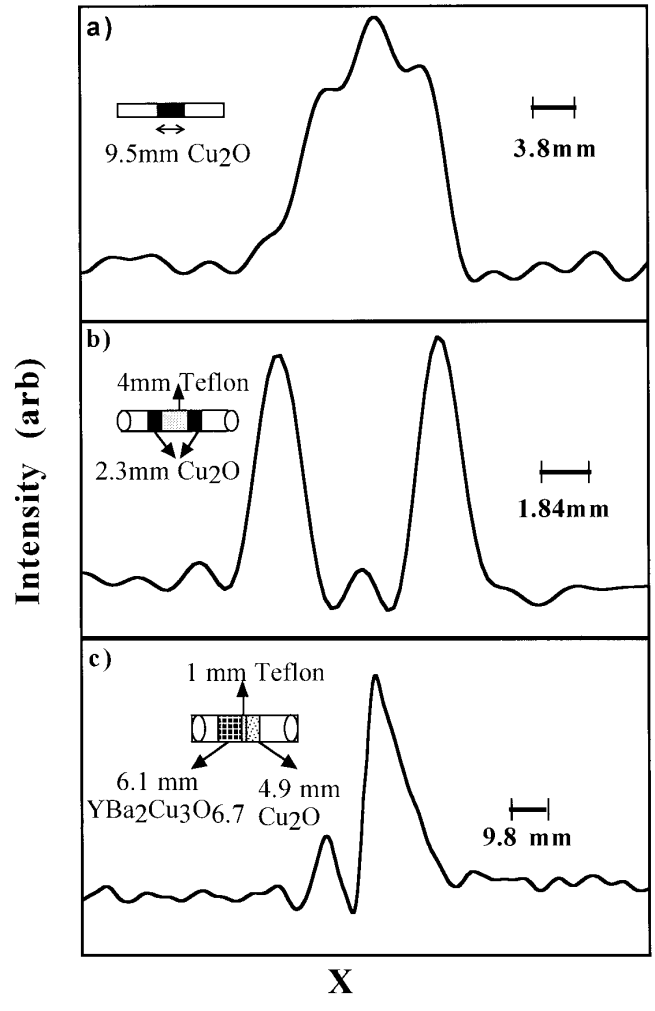

FIG. 4. Experimental 1D projections at 96.2 MHz of (a) single-piece phantom of 9.5-mm-long Cu_2O powder ($\nu_Q^2/\nu_L^2 = 0.0738$), (b) two-piece phantom of 2.3-mm-long Cu_2O powder with a 4-mm gap in between, (c) two-piece phantom of 4.9-mm-long Cu_2O (+ chalk dust), 6.1-mm-long HTSC ($YBa_2Cu_3O_{6.7}$), with a 1-mm gap in between.

In fact we have demonstrated this to a limited degree in the measurements presented here by choosing a frequency far from that of the copper metal signal from the coils. In a more elaborate measurement, images can be acquired at several well-separated frequencies analogous to multispectral methods used in remote sensing applications.

CONCLUSION

Simulations were developed for the extra image broadening due to the presence of a large electric quadrupole interaction. The broadening is found to be proportional to the sample size, but for smaller samples one can still get good resolution even for severely broadened spectra such as those of Cu_2O and $YBa_2Cu_3O_{6.7}$. Using a simple phase encoding scheme the measurements, though tedious, are indeed feasible as is demonstrated by experimental results for samples of Cu_2O and $YBa_2Cu_3O_{6.7}$. For even larger EFGs, the simple phase encoding scheme cannot be expected to yield good results.

ACKNOWLEDGMENTS

The authors thank M. Ming for the data in Fig. 2 and Boyd W. Veal of Argonne National Labs for the HTSC material.

REFERENCES

1. A. Abragam, in ''Principles of Nuclear Magnetic Resonance,'' edited by D. W. W. C. Marshall, pp. 216–263. Clarendon, Oxford (1992).
2. B. H. Suits and D. White, *Solid State Commun.* **50**(4), 291 (1984).
3. B. H. Suits and J. L. Lutz, *J. Appl. Phys.* **65,** 3728 (1989).
4. B. H. Suits, *Mat. Res. Soc. Symp. Proc.* **217,** 67 (1991).
5. M. S. Conradi, *J. Magn. Reson. A* **93,** 419 (1991).
6. G. H. Stauss, *J. Chem. Phys.* **40,** 1988 (1964).
7. T. P. Das and E. L. Hahn, in ''Solid State Physics, Supplement 1, Nuclear Quadrupole Resonance Spectroscopy,'' edited by F. Seitz and D. Turnbull. Academic Press, London (1958).
8. M. H. Cohen and F. Reif, *Solid State Phys.* **5,** 321 (1957).
9. N. B. Bloembergen and T. J. Rowland, *Acta Met.* **1,** 731 (1953).
10. B. H. Suits and D. E. Wilken, *J. Phys. E: Sci. Instrum.* **22,** 565 (1989).
11. B. H. Suits and G. Y. Plude, *J. Magn. Reson. A* **117,** 84 (1995).
12. A. Kumar, D. Welti, and R. R. Ernst, *J. Magn. Reson.* **18,** 69 (1975).
13. E. E. Anderson, ''Modern Physics and Quantum Mechanics,'' pp. 342–343. Saunders, Philadelphia (1971).
14. R. E. Walstedt, in ''Pulsed Magnetic Resonance: NMR, ESR and Optics, A Recognition of E. L. Hahn,'' edited by D. M. S. Bagguley, pp. 242–259. Clarendon, Oxford (1992).
15. M. S. Conradi, A. N. Garroway, D. G. Cory, and J. B. Miller, *J. Magn. Reson.* **94,** 370 (1991).
16. M. J. E. Golay, *Rev. Sci. Instrum.* **29,** 313 (1958).
17. M. J. E. Golay, Ger. Offen Patent Number 1,946,059 (1970).
18. H. Krüger and U. Meyer-Berkhout, *Z. Physik* **132,** 171 (1952).
19. M. Mali, D. Brinkmann, L. Pauli, J. Roos, H. Zimmermann, and J. Hulliger, *Phys. Lett. A* **124,** 112 (1987).
20. E. A. Hill and J. P. Yesinowski, *J. Am. Chem. Soc.* **118,** 6798 (1996).
21. E. A. Hill and J. P. Yesinowski, *J. Chem. Phys.* **106,** 8650 (1997).